Hindawi
Journal of Nanomaterials
Volume 2022, Article ID 3167809, 14 pages
https://doi.org/10.1155/2022/3167809

Research Article

Tin Oxide/Nitrogen-Doped Graphene Quantum Dots Composite Nanotubes: An Efficient Electrode for Supercapacitors

Seshendra Reddy Ch,[1] Ravindra N. Bulakhe,[2,3] Jeevan Kumar Reddy Modigunta,[2] G. Murali,[2] Reddy Sivasankar A.,[1] Jiyeong Kim,[2] Eunji Park,[2] Byungin Kang,[2] Insik In,[2] Arup Kumer Roy,[4] Kiruthiga Ramakrishnan,[5] and Udayabhaskar Rednam[5]

[1]*Department of Physics, Vikrama Simhapuri University P.G. Centre, Kavali, 524201 Andhra Pradesh, India*
[2]*Department of Polymer Science and Engineering, Department of IT-Energy Convergence (BK21 FOUR), Chemical Industry Institute, Korea National University of Transportation, Chungju 27469, Republic of Korea*
[3]*Soft Energy Systems and Laser Applications Laboratory, School of Mechanical Engineering, Chung-Ang University, Seoul 06974, Republic of Korea*
[4]*Department of Chemistry, Chittagong University of Engineering & Technology, Chittagong-4349, Bangladesh*
[5]*Instituto de Investigaciónes Científicas Y Tecnológicas (IDICTEC), Vicerrectoría de Investigación Y Postgrado, Universidad de Atacama, Avenida Copayapu, 485 Copiapó, Chile*

Correspondence should be addressed to Arup Kumer Roy; arupkumer@cuet.ac.bd

Received 10 September 2021; Revised 28 December 2021; Accepted 23 May 2022; Published 13 July 2022

Academic Editor: Antonios Kelarakis

Tin oxide (SnO_2) and nitrogen-doped graphene quantum dots (N-GQDs) composite nanotubes (SnO_2/N-GQD NTs) were fabricated by the electrospinning technique and followed by the thermal annealing method for the application in supercapacitor as an electrode. SnO_2/N-GQD NTs with different ratio of N-GQDs were prepared by adding different ratios of N-GQDs along with tin chloride during the electrospinning process. The prepared composite's structure and morphological properties were characterized by using different techniques like XRD, FE-SEM, TEM, and XPS. The supercapacitor performance of the SnO_2/N-GQD NTs composite was analyzed by the electrochemical studies such as cyclic voltammetry and galvanostatic charge-discharge (GCD) measurement in 2 M KOH solution as electrolyte. The electrochemical analyses of SnO_2/N-GQD NTs was tested at different scan rates and current densities. SnO_2/N-GQD NTs prepared using 3 wt.% of N-GQDs showed an excellent capacity retention even after 5000 GCD cycles and exhibited a maximum specific capacitance of 420 mF g^{-1} at a current density of 8 mA cm^{-2} in comparison to pure SnO_2 NTs (230 mF cm^{-2}).

1. Introduction

In the past few decades, the continuous growth in the demand for energy thrived researchers to find an alternative energy storage and conversion systems for the depleting fossil fuels which are affecting the global environment. Among various available energy storage and conversion devices, such as batteries, fuel cells, and supercapacitors (SCs), SCs provide an instant high-power density for the required applications [1–5]. SCs have gained a wide attention in the interdisciplinary fields due to their amazing characteristics like, high efficiency at prolonged cycles [6], high-power density, and high-energy density [7, 8]. In general most of the metal oxide semiconductors (MOS) such as RuO_2 [9, 10], NiO [11], SnO_2 [12], MnO_2 [13, 14], Fe_3O_4 [15], CuO [16], ZnO [17], and CoO [18] are having a significant contribution for the SC applications [19]. Tin oxide (SnO_2) is well-known among MOS due to its vast applications such as in gas sensors [20, 21], biosensors [22, 23], solar cells [24, 25], Li-ion battery materials [26, 27], photocatalytic applications [28],

and SCs [29, 30]. Among the MOS, SnO_2 is a non-toxic and easily synthesizable nanomaterial [31]. Although SnO_2 performs well for SCs, the limiting factors such as poor electrical conductivity, poor transportation of electrolyte ions within the SnO_2 matrix, and huge volume expansion hinder its practical applicability [32]. In order to improve SnO_2 as an efficient electrode material for the SCs, the combination of SnO_2 with other conductive materials containing a high surface area and good morphologies is one of the most suitable choices. The composites made of a conductive material such as carbon-based materials with SnO_2 and related composites are one of the good choices among many available methods in order to enhance the performance as electrode for SCs.

In recent years, carbon-based materials are among the eco-friendly, low-cost, and easily available sources for improving the conductivity of MOS along with different morphologies with high surface area [33]. Carbon-based nanomaterials and MOS nanocomposites have been reported to be good electrode materials for energy conversion and storage applications [26, 34]. The preparation of 2D fiber or tube-like morphologies supports the improvement of internal conductivity in the materials which contains interconnecting branching networks in the structures. These type of morphologies can be easily fabricated using the electrospinning method [35].

The composites of carbon-based materials contribute to the improvement of the pseudocapacitance of the materials in electrochemical analysis. In recent times, heteroatom-doped carbon-based materials such as N-doped graphene and N-doped graphene quantum dots (N-GQDs) are among the carbon nanostructures that have been studied majorly [36–38]. N-GQDs are used as the electrodes for SCs and found that they exhibited superior capacitance and rate performance [39]. These properties make N-GQDs as one of the suitable materials for making composites with MOS for improving the electrochemical performance. The fabrication of these nanotube (NT) composite materials with nanometer scale morphology is one of the challenging processes to obtain a highly active sites and good conductive networks. However, the N-GQDs incorporated SnO_2 NTs can be a good suitable electrode material for the improvement of electrochemical performance of SnO_2 in SC applications.

In this work, the SnO_2 NTs and SnO_2/N-GQD NTs have been prepared by two-step process in which first the solution of tin chloride and N-GQDs (with 3 and 5 wt.%) along with polyvinylpyrrolidone in DMF solutions was subjected to electrospinning followed by thermal annealing. This process is cheaper, easy to handle, and has the advantage of easy morphological control. The electrochemical performance of synthesized SnO_2/N-GQD NTs was studied by fabricating a SC device with a three-electrode system configuration and aqueous potassium hydroxide as electrolyte.

2. Experimental

2.1. Materials. Tin (II) chloride dihydrate ($SnCl_2{\cdot}2H_2O$), *N*, *N*-dimethylformamide (DMF), ethanol, polyvinylpyrrolidone (PVP, $M_w = 1{,}300{,}000\,\mathrm{g\,mol^{-1}}$), citric acid monohydrate, urea, polyvinylidene fluoride (PVdF), and N-methyl pyrrolidone (NMP) were procured from Sigma Aldrich, USA. Conductive additive super p carbon and Ni-foam were procured from MTI Corporation, South Korea. All the chemicals purchased were used as received without any further purification.

2.2. Synthesis of N-GQDs. Citric acid monohydrate (0.42 g) and urea (0.36 g) were mixed in 12 mL deionized water and sonicated for 60 min. The mixture was then transferred to a Teflon-lined autoclave (50 mL) and heated at 180 °C for 3 h. After cooling the autoclave to room temperature, the resultant product was filtered and washed with ethanol and centrifuged at 8000 rpm for 5 min. The solid precipitate obtained was dried at 50 °C for 10 h to obtain the nitrogen-doped graphene quantum dots (N-GQDs) [38].

2.3. Synthesis of SnO_2 Nanotubes and N-GQD Incorporated SnO_2 Nanotubes. $SnCl_2{\cdot}2H_2O$ (0.7 g) was dissolved in 4.2 mL ethanol and sonicated adequately for 1 h; simultaneously, 0.44 g of PVP was dissolved in DMF and stirred for 3 h. Finally, both clear solutions were mixed and stirred for 4 h to obtain the precursor liquid for electrospinning. N-GQDs (3 and 5 wt.%) incorporated tin chloride NTs were prepared by adding the solution of tin chloride with pre-prepared N-GQD solution with stirring for several hours until the solution becomes uniform. The obtained solution was loaded into the syringe and electrospinned. For the preparation of the pristine tin chloride and N-GQD incorporated tin chloride NTs, a constant voltage of 12 kV and 15 kV was applied, respectively. The distance between the syringe needle and the electrospun mat collector was fixed at 12 cm. The specimens were collected and dried in vacuum oven for overnight. Pure SnO_2 and N-GQDs incorporated SnO_2 nanotube composites were obtained by annealing the dried electrospun mats at 600 °C for 2 h and 500 °C for 4 h, respectively. The samples were denoted as S1 for pure SnO_2 NTs, S2 for SnO_2 NTs with 3 wt.% of N-GQDs, and S3 for SnO_2 NTs with 5 wt.% N-GQDs-loaded samples. The detailed synthesis procedure is shown in Scheme 1.

2.4. Materials Characterization. The structural properties of the prepared samples (S1, S2, and S3) were characterized by the patterns obtained from X-ray diffraction (Bruker, D8 ADVANCE, USA). The surface morphology and microstructure of the samples were characterized by field emission scanning electron spectroscopy (FE-SEM, JEOL, JSM-6700F, Japan) and transmission electron microscopy (TEM, Tecnai G2 F20, FEI Corporation, Japan). The chemical bonds in the samples were characterized using X-ray photoelectron spectra (XPS, Scientific Sigma Probe Multi-2000 spectrometer, Thermo VG Scientific Co., USA).

2.5. Electrochemical Characterization. The electrochemical analyses were carried by using a Ni foam electrode coated with the prepared active materials. For electrode preparation, 80 wt.% active material, 10 wt.% polyvinylidene fluoride (PVDF) and 10 wt.% conductive carbon were mixed in n-methyl-2-pyrrolidone (NMP). The mixture was made as fine slurry, and then, it was coated on Ni foam (1 × 4 cm) in

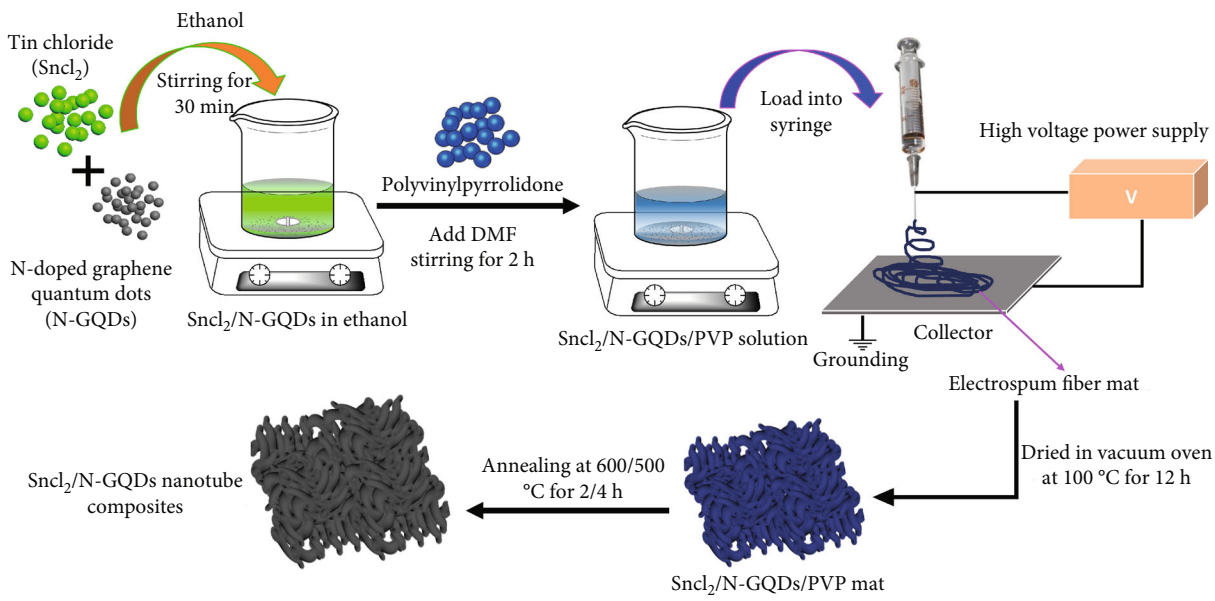

Scheme 1: Schematic diagram for the synthesis of SnO_2 nanotubes and N-GQDs incorporated SnO_2 nanotubes by electrospinning followed by thermal annealing.

1×1 cm size and then dried in vacuum oven for 12 h at 100 °C. The loading of the active material in the electrodes is approximately 2.5 mg cm^{-2}. Electrochemical measurements such as cyclic voltammetry (CV) and galvanostatic charge–discharge (GCD) were performed at room temperature with the help of Wonatech, Korea, instrument using three-electrode configuration in 2 M KOH electrolyte solution. Electrochemical impedance spectra (EIS) analyses were performed using frequency range between 0 Hz and 50 kHz. CV was carried out at various scan rates (5 to 100 mV/s) in the potential window of 0-0.5 V. GCD was performed at different current densities (1 to 8 mA g^{-1}) in the voltage window of 0-0.5 V. The specific capacitance of the SCs is calculated by using the formula:

$$\text{Specific capacitance}\left(C_{sp}\right) = \frac{I \times \Delta t}{m \times \Delta V}, \quad (1)$$

where $I\,(A)$ is discharge current, $\Delta t\,(s)$ is the discharge time consumed for in the potential range of V, $m\,(g)$ is the mass of the active material, and $\Delta V\,(V)$ is the potential window used for the charge-discharge. Energy density and power density of the fabricated materials are determined by using the following equations:

$$\text{Energy density}(E) = \frac{C_{sp} \times \Delta V^2}{2}, \quad (2)$$

where C_{sp} (F g^{-1}) is the specific capacitance calculated from charge-discharge process and ΔV is the potential window used in the charge-discharge process.

$$\text{Power Density}(P) = \frac{E}{\Delta t}, \quad (3)$$

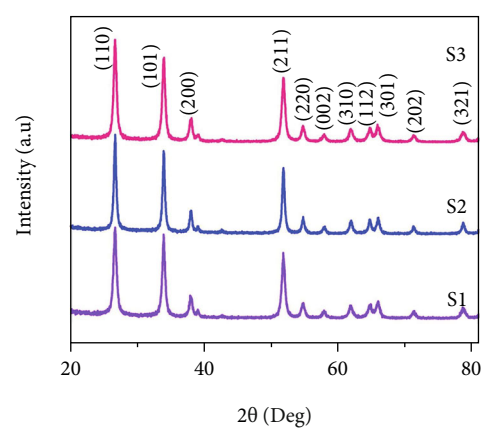

Figure 1: XRD spectral data of S1 (SnO_2) nanotubes, S2 (SnO_2/N-GQDs-3 wt.%) nanotubes, and S3 (SnO_2/N-GQDs-5 wt.%) nanotubes.

where E is the energy density calculated from the specific capacitance and Δt discharge time of the supercapacitor.

3. Results and Discussions

Figure 1 Shows the XRD patterns of S1, S2, and S3 NTs with the major peaks corresponding to the (110), (101), (200), (211), (220), (002), (310), (112), (301), (202), and (321) lattice planes of the rutile structure of SnO_2. XRD patterns are in good agreement with the reference patterns of SnO_2 with JCPDS number 41-1445, which are compatible with previous reports [40]. The lack of N-GQD peaks in XRD might be due to the dominant concentration of the SnO_2 matrix in the samples. The effect of N-GQDs incorporation into the samples is studied by considering the (110) diffraction peak as reference candidate to calculate the crystallite

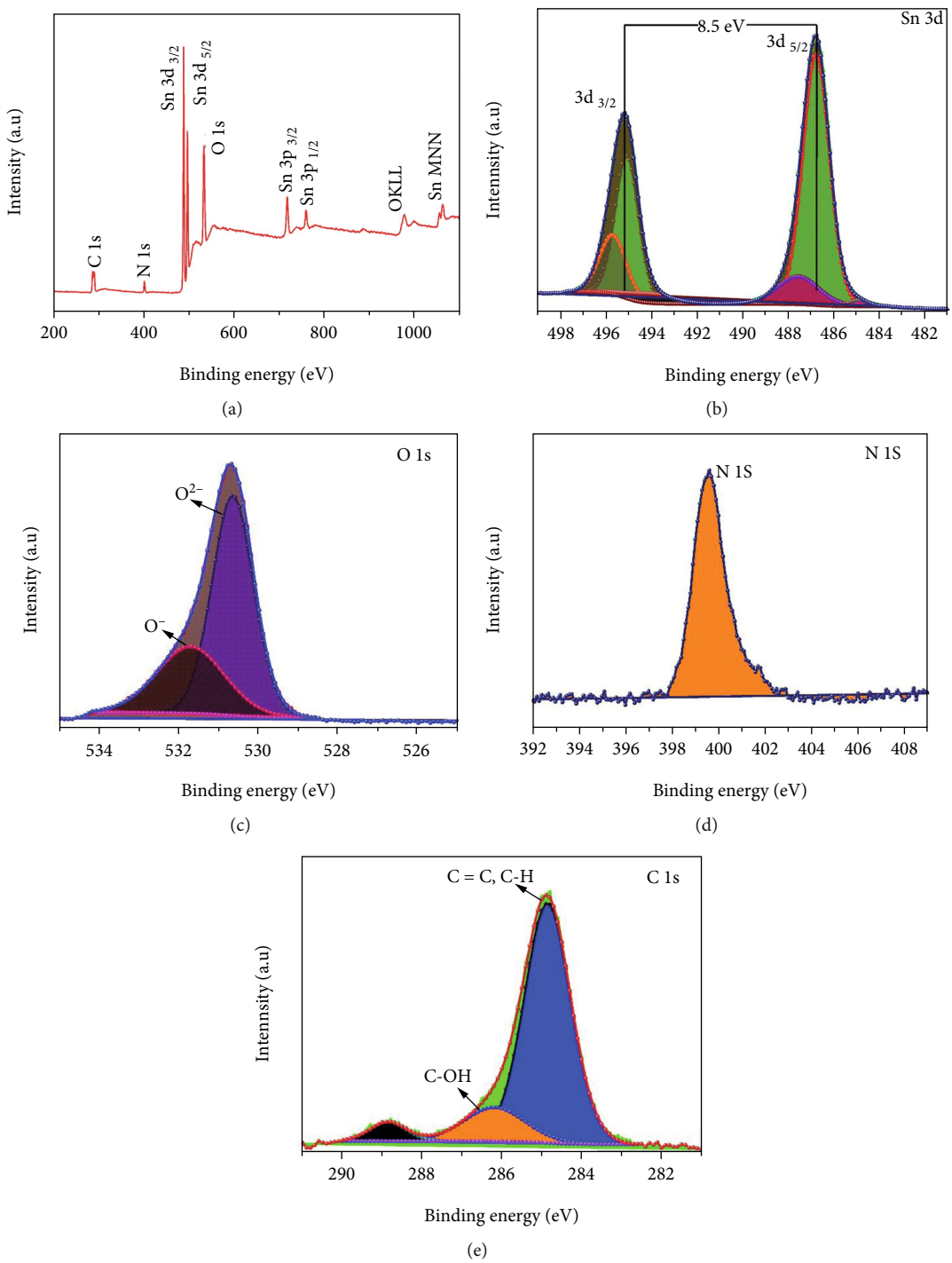

Figure 2: XPS (a) survey scan spectrum and high resolution deconvoluted spectra for (b) Sn 3d, (c) O 1s, (d) N 1s, and (e) C 1s, of sample S2 (SnO_2/N-GQDs-3 wt.%).

size. The crystallite size of the samples is calculated using the Scherrer's formula. The calculated average crystallite size of the S1, S2, and S3 are 10.1 nm, 12.3 nm, and 14.5 nm, respectively, showing change in the crystallite size caused by the N-GQDs incorporation during the synthesis process.

The surface elemental composition of the S2 is analyzed by XPS as shown in Figure 2. The survey scan spectrum (Figure 2(a)) detected elements Sn, C, N, and O. The peaks of Sn 3d, Sn 3p, and MNN were detected from SnO_2. The Sn 3d ($3d_{3/2}$ and $3d_{5/2}$) peaks were observed at 495.2 and 486.7 eV (Figure 2(b)) corresponding to Sn^{4+} in the rutile SnO_2 structure. In Figure 2(c), the O 1s spectra of the S2 shows the peaks at 532.1, 531.2, and 530.4 eV; corresponding to oxygen absorption (O_2^-), oxygen vacancy (O^-), and oxygen binding (O_2^-), this designates the formation of oxygen vacancies in S2. XPS spectra of the S2 sample have an obvious peak at 399.8 eV corresponding to N 1s (Figure 2(d)) due to the presence of nitrogen functional groups (from N-

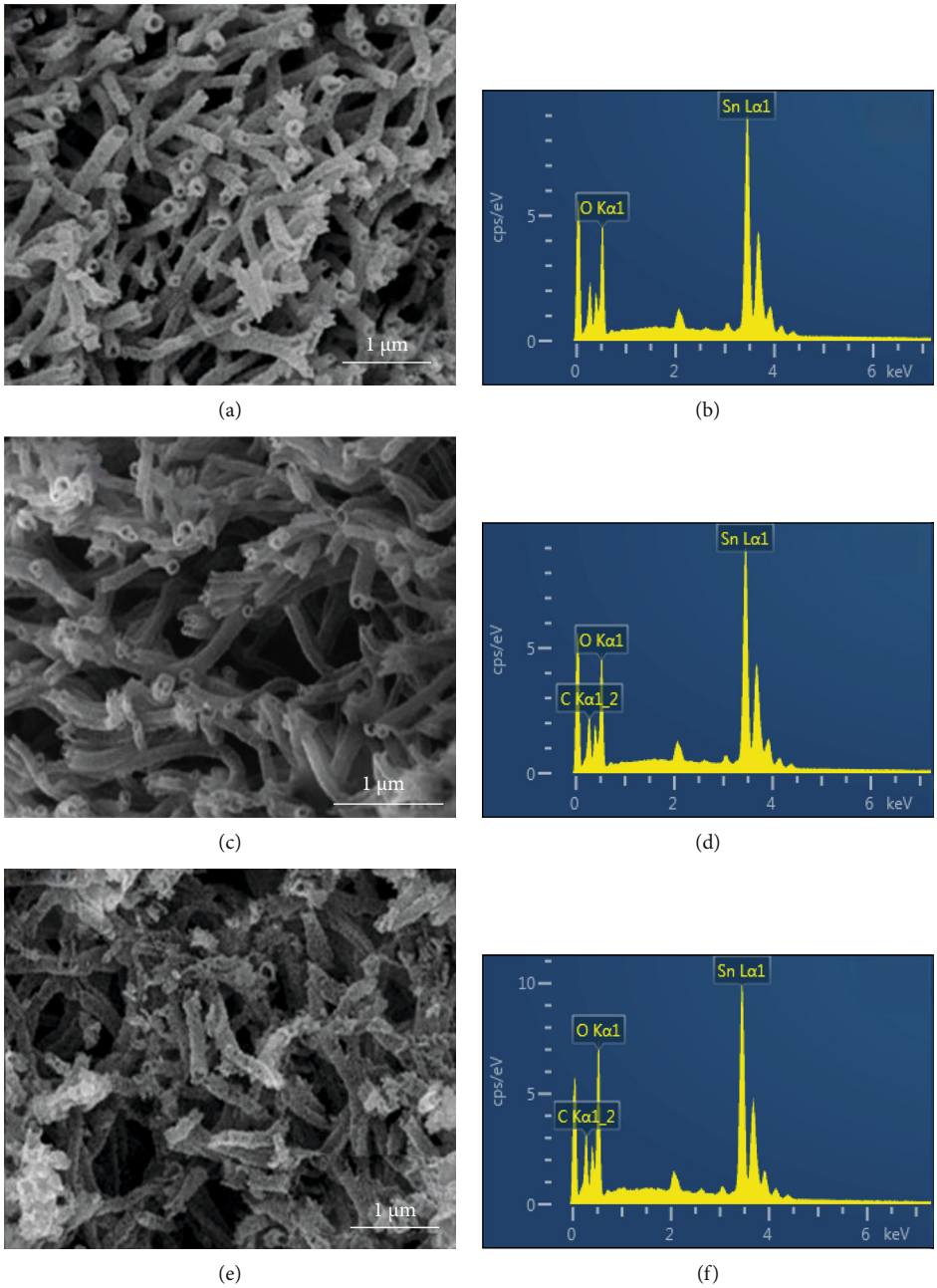

Figure 3: FE-SEM images and EDS spectrum of samples (a, b) S1 (pure SnO_2 nanotubes), (c, d) S2 (SnO_2/N-GQDs-3 wt.% nanotubes), and (e, f) S3 (SnO_2/N-GQDs-5 wt.% nanotubes).

GQDs). The peak of C1s can be attributed mainly to GQDs as shown in Figure 2(e). The C1s spectrum shows a strong peak center at 284.9 eV that is attributed for the C=C/C–C bonds, and peaks at 285.5 and 286.7 eV revealing the presence of C=N (sp^2) and C–N (sp^3) bonds, respectively. The XPS analysis provides evidence for the formation of N-doped GQDs and their composites in combination with SnO_2 [41].

FE-SEM and EDS spectral images of S1, S2, and S3 NTs are shown in Figures 3(a)–3(f). In all samples, NTs are randomly oriented in all directions with the rough surface. Figures 3(a)–3(b), Figures 3(c)–3(d), and Figures 3(e)–3(f) represent the FE-SEM images and EDS spectra of S1, S2, and S3 samples after calcination, respectively. The elemental composition of pristine and composite SnO_2 NTs is determined by EDS analysis that indicates the presence of Sn, O, and C elements as shown in Figure 3. Pristine and N-GQDs incorporated SnO_2 long NTs are having the diameter in the range of 15–40 nm. From FE-SEM and EDS results, it is observed that almost there were no trances of PVP-based amorphous carbon after thermal annealing. Although PVP created some porous vacancies during the annealing process, the nanotube structures were retained during the calcination process due to the crystallization of SnO_2. From FE-SEM images, it can also be observed that the S1 and S2 are thin and almost uniform. In the case of S3 sample, as the N-

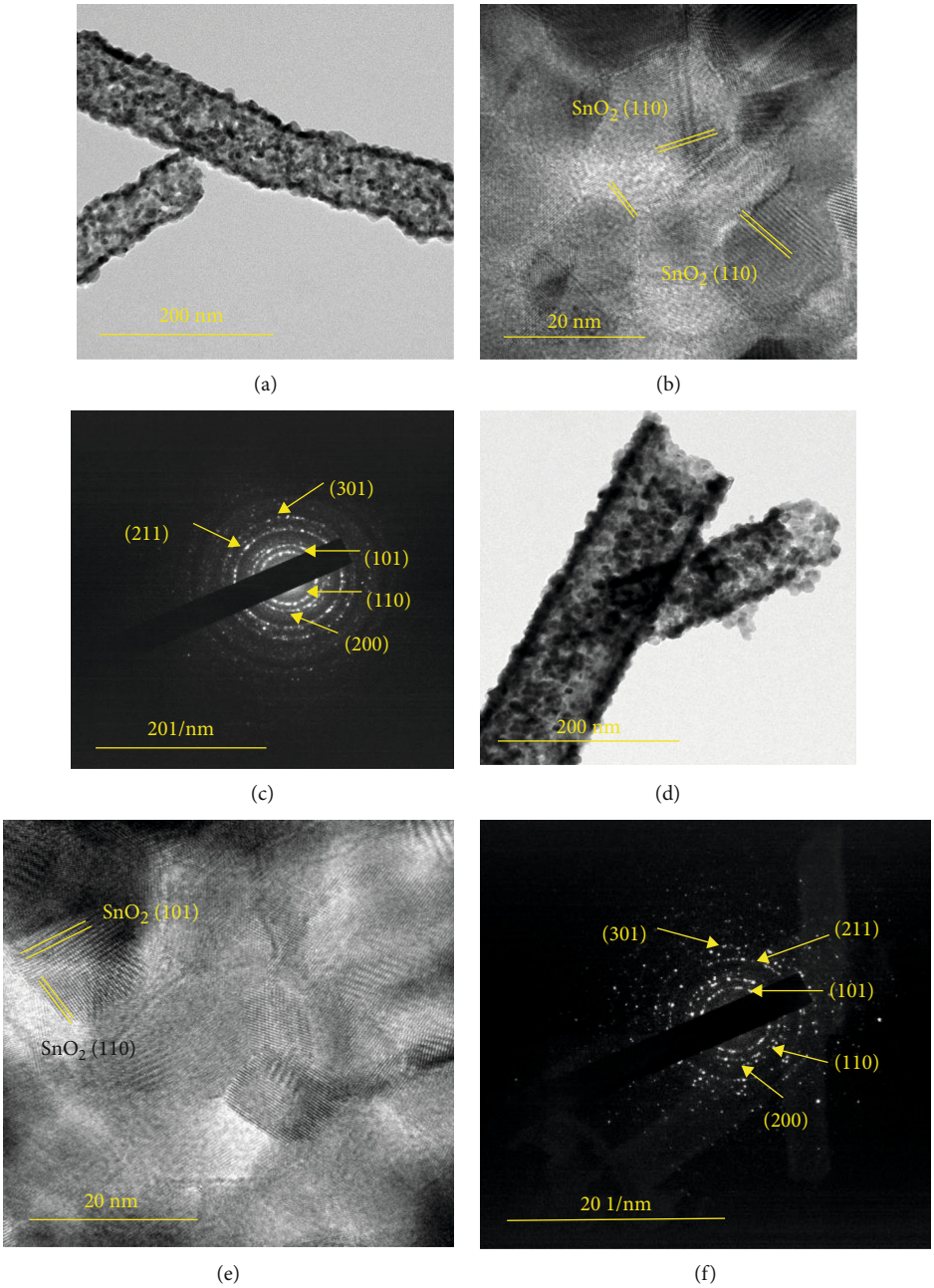

Figure 4: TEM, HR-TEM, and SAED pattern images of (a–c) SnO_2 (S1) and (d–f) SnO_2/N-GQDs composite material (S2).

GQDs concentration is about 5 wt.%, the NTs were broken, and this may be due to the increase in the viscosity of the electrospinning precursor solution.

Figure 4 shows the TEM, HR-TEM, and SAED images of S1 and S2 samples. Figures 4(a)–4(c) display the TEM, HR-TEM, and SAED images of S1, i.e., pristine SnO_2 NTs. The size of pristine SnO_2 nanoparticles is about 20 nm. The nanoparticle network has been continued in the form of nanotube by the mutual sharing of the crystal edges of each particle. The crystal structure of S2, i.e., SnO_2/N-GQD NTs (Figures 4(d)–4(f)), could be verified in the high-resolution TEM. The SnO_2 NTs consist of crystalline nanoparticles-shaped SnO_2, and the N-GQDs were tightly incorporated in the SnO_2 NTs. Moreover, the HR-TEM images demonstrate clear lattice fringes with *d*-space of 0.34 nm and 0.27 nm, which are in good agreement with that of the (101) and (110) planes of SnO_2. The SAED images of the S1 and S2 represent the monocrystalline structure and that is in good agreement with the XRD analysis as discussed earlier.

The electrochemical analysis of the prepared samples was investigated using CV, EIS, and GCD cycling through a three-electrode configuration. In the three-electrode system devices, active material-loaded Ni foam is used as working electrode, Ag/AgCl as the reference electrode, and platinum strip as

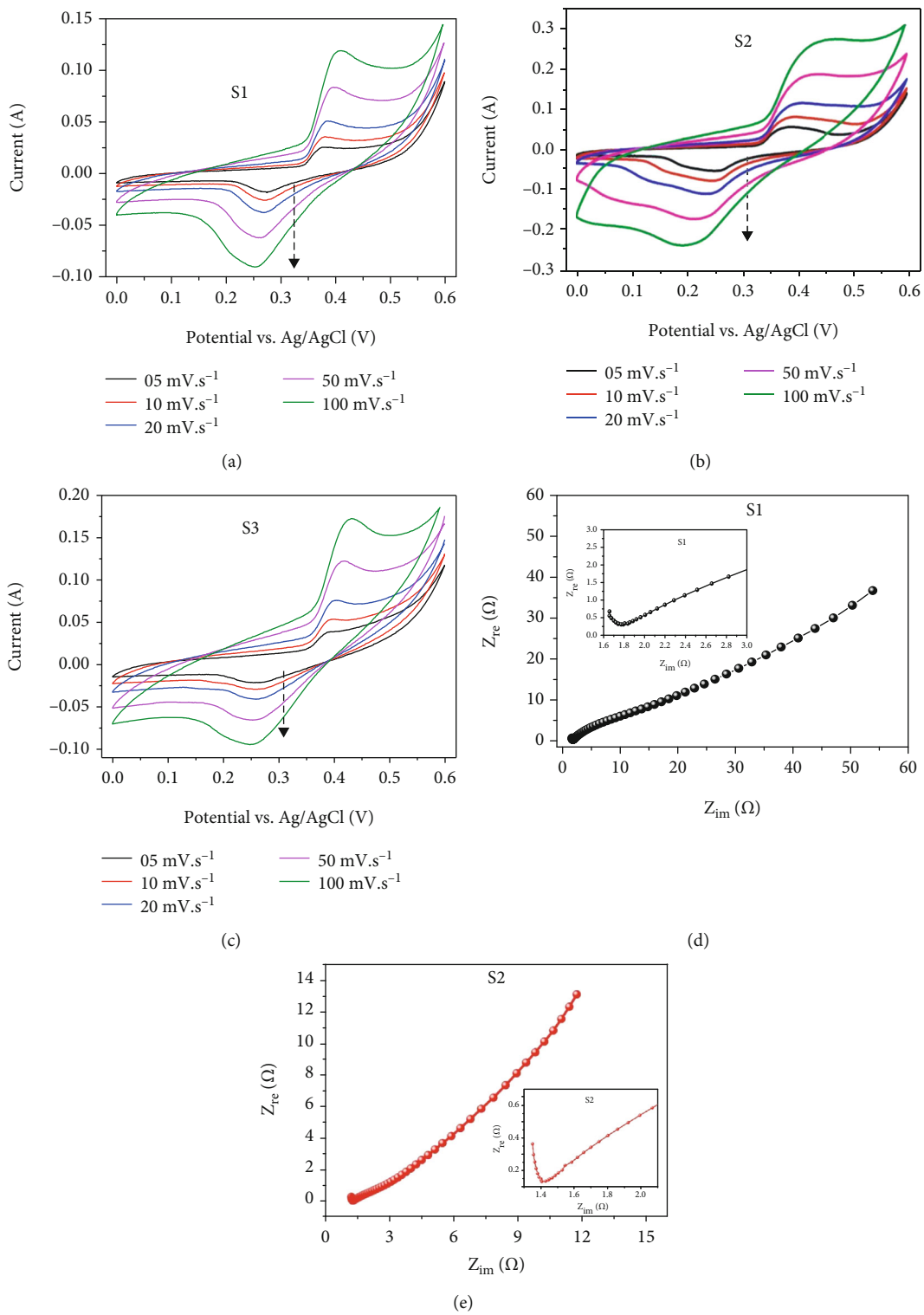

Figure 5: Continued.

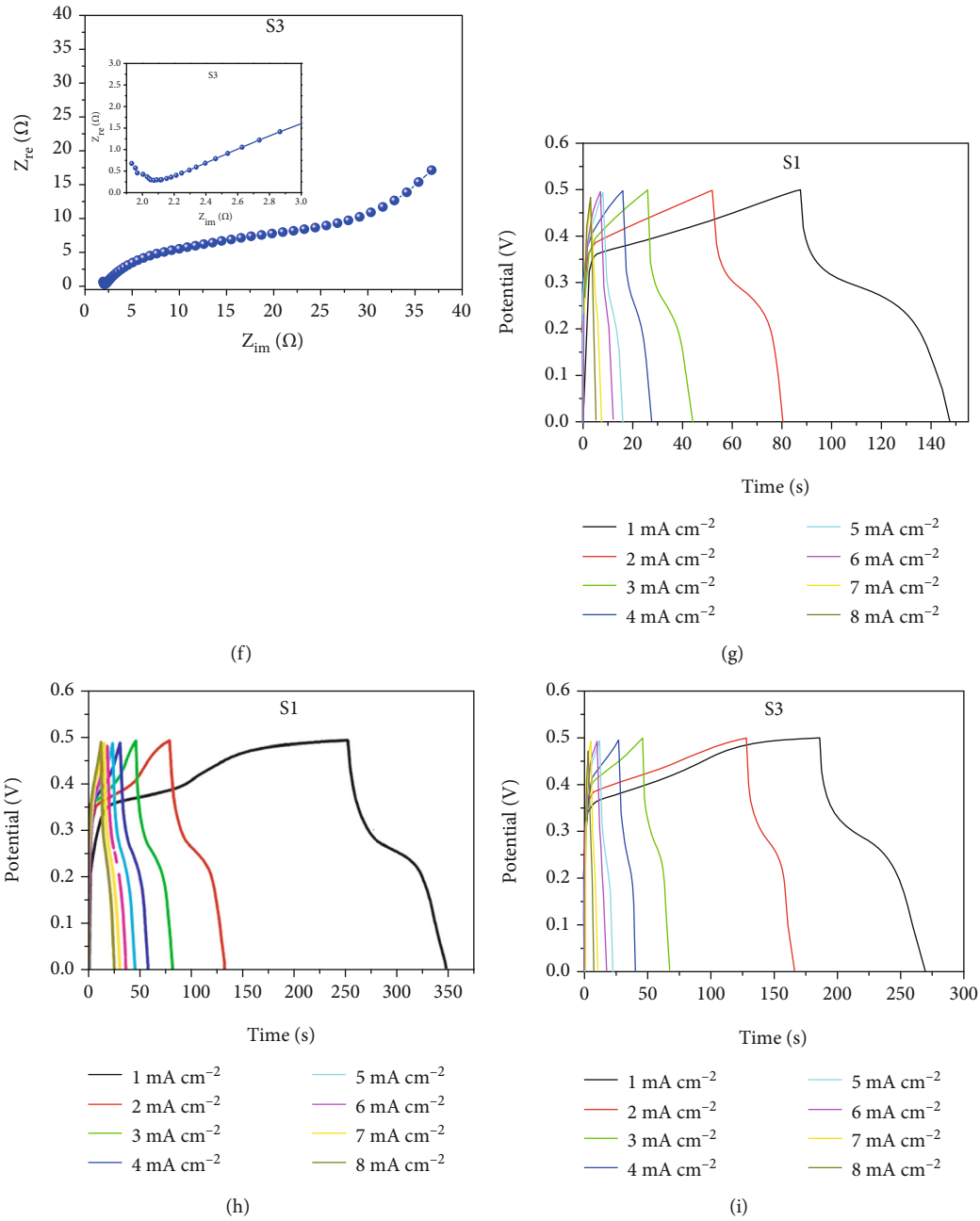

Figure 5: Electrochemical performance evolution of the S1, S2, and S3 electrodes: (a–c) cyclic voltammetry (CV) curves at different scan rates from 5 to 100 mV s^{-1}, (d–f) Nyquist plots (EIS) analyzed in the frequency range 0.1 to 10 kHz (inset, selective magnified scale in the high-frequency region), and (g–i) galvanostatic charge-discharge (GCD) curves at different current densities from 1 to 8 mA cm^{-2}.

counter electrode. Aqueous 2 M KOH was used as the electrolyte for the analyses. The CV, EIS, and GCD analysis results for S1, S2, and S3 are shown in Figure 5.

Figures 5(a)–5(c) show the CV curves of S1, S2, and S3 electrodes for comparison in the potential window of 0 to 0.6 V in 2 M KOH aqueous electrolyte at different scan rates from 5 to 100 mV s^{-1}. CV curves of S1, S2, and S3 have shown noticeable redox peaks at ~0.38 and 0.27 V. The CV curve for S1 electrode has clearly shown the characteristic redox peaks for SnO_2 material (Figure 5(a)). The CV curves of S2 has shown well-defined redox peaks similar to S1, indicating the presence of quasi-reversible faradaic reactions at different scan rates as shown in Figure 5(b). The redox peaks of S2 sample are broadened with increase of the scan rate from 5 to 100 mV s^{-1} might be due to the fact that the quasi-reversible redox reactions at the surface of SnO_2 material along with the conductive N-GQDs in the electrodes that might help to enhance the internal conductivity of the electrodes. Whereas in the case S3 electrode, the CV redox peak positions were similar to the previous electrodes, but the peak broadening was not observed as that of S2 (Figure 5(c)). The possible redox reactions of the SnO_2/N-GQD NT electrodes during the CV process (between Sn(III)/

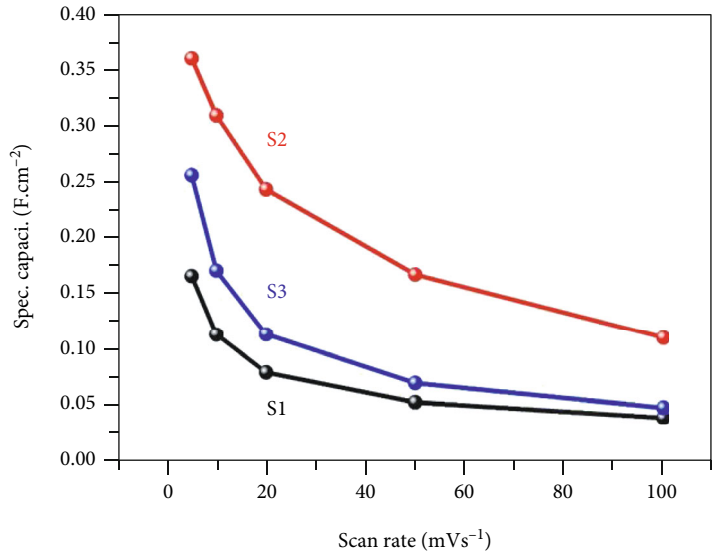

(a)

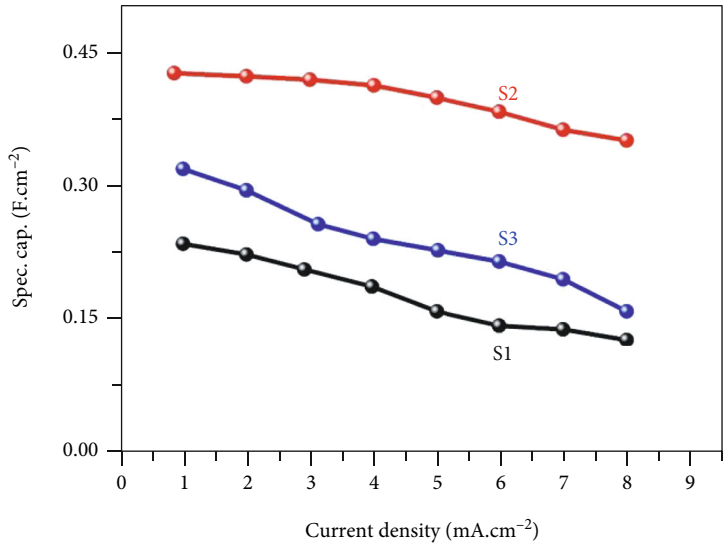

(b)

Figure 6: Continued.

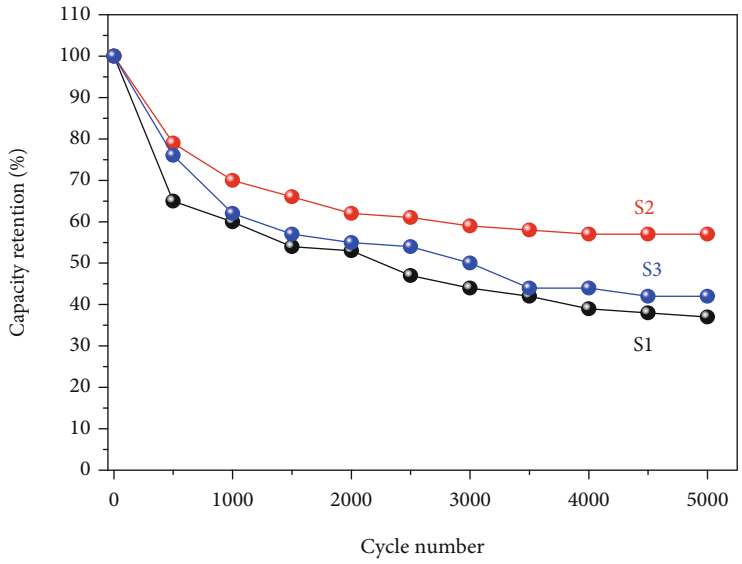

(c)

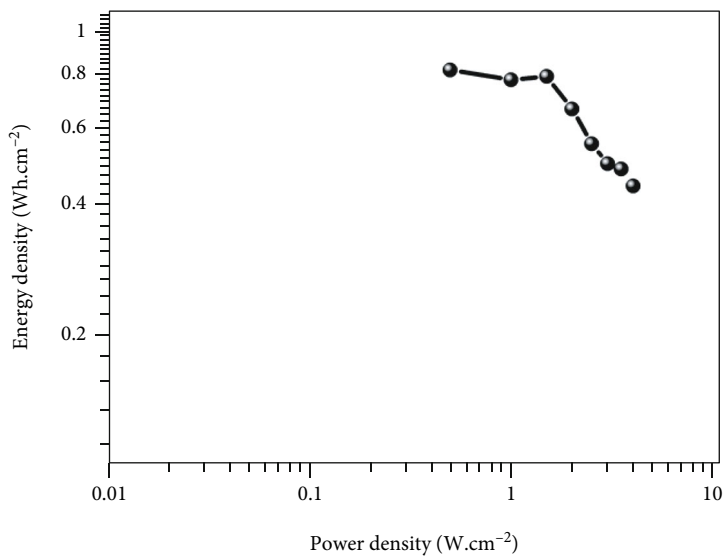

(d)

Figure 6: Electrochemical performance of S1 (SnO_2 NTs), S2 (SnO_2/N-GQD-3 wt.% NTs), and S3 (SnO_2/N-GQD-5 wt.% NTs) electrodes: (a) specific capacitance vs. scan rate, (b) plots of specific capacitance vs. current density, and (c) capacity retention efficiency with respect to cycle number. (d) Ragone plot of energy density vs. power density for supercapacitor with S2 electrodes.

Sn(IV) in reaction with OH^-) are described in Equations (4) and (5) [42].

$$SnO_2 + OH^- \leftrightarrow SnOOH + e^- \quad (4)$$

$$SnOOH + OH^- \leftrightarrow SnO_2 + H_2O + e^- \quad (5)$$

The electron/ion transport behavior of the nanocomposites is understood by using EIS measurements. EIS measurements also carried to compare the resistance at the interface of the electrode materials interface and the electrolyte in the devices fabricated using electrodes made-up of S1, S2, and S3 materials as shown in Figures 5(d)–5(f). The Nyquist plots of the nanocomposites were showing the semi-half circle followed by the immediate raise in the diffusion resistance in the high-frequency region (as shown in the inset of Figures 5(d)–5(f)) and a linear slope in the low-frequency region. The charge transfer resistance (R_{ct}) was observed for all the samples, and the inclined line is attributed to the anomalous diffusion of the ions in the electrolyte to the modified electrode. The R_{ct} of the electrodes indicates the presence of more resistance due to the semiconducting SnO_2 in S1, whereas the R_{ct} value decreases for S2 electrodes and further increases for S3 as shown in Figures 5(d)–5(f). The device with S2 electrode showed a least resistance in comparison to S1 and S3. The above electrochemical results imply that S2 electrode is a high

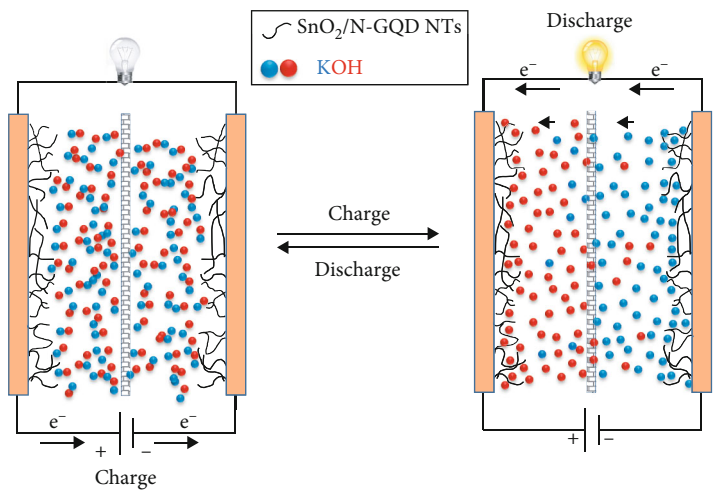

Figure 7: The schematic of the possible mechanism involved in the SnO_2/N-GQD NT composite electrodes during the charge-discharge processes.

potential candidate for the application of SCs in comparison to the S1 and S3 electrodes.

The N-GQDs will not take part in the redox reaction directly, and it will enhance the electrical/ionic conductivity of the composites with faster kinetics of positive ions during the redox process by means of electric double layer (EDL) formation. The GCD profiles of S1, S2, and S3 electrodes at different current densities ranging from 1 to 8 mA cm^{-2} are shown in Figures 5(g)–5(i). The corresponding areal capacitance values at different current densities were calculated, and the results were compared for S1, S2, and S3. The areal capacitances of the S2 electrode are calculated at different current densities from 1 to 8 mA cm^2 and are varying from 420 to 200 mF cm^{-2}, respectively, as shown in Figure 5(h). S2 electrode delivers higher areal capacitance of 420 mF cm^{-2} at current density of 1 mA cm^{-2}, as compared to S1 (230 mF cm^{-2}) and S3 (320 mF cm^{-2}) as shown in Figures 5(g)–5(i). The S2 electrode revealed good electrochemical performance in comparison to S1 and S3 electrodes; this might be due to the improved conductivity of the S2 electrode. The CV curves with redox peaks and charge-discharge plots with lower internal resistance indicate that the materials are suitable for SC applications.

Figure 6(a) shows the specific capacitance of the electrodes S1, S2, and S3 with respect to scan rates used in the CV analysis. Similarly, Figure 6(b) shows the specific capacitance with change in current densities varied from 1 to 8 mA cm^{-2}. From these electrochemical analyses, it can be corroborated that electrodes prepared using S2 sample are having the best possible combination of N-GQDs and SnO_2 NTs for the application in SCs.

The specific capacitance is decreased at higher scan rates, which could be due to the approach of positive ions (K^+) only at the outer surface of the electrode during the EDL formation and/or quasi-reversible reactions. Whereas at lower scan rates, positive ions could easily diffuse into all the available spaces of electrode, thus leading to sufficient insertion reaction to form quasi-reversible reactions and/or EDL formation or to show a high specific capacitance [43, 44]. The capacitance retention of S1, S2, and S3 electrodes studied by the GCD measurements at 10 mA cm^{-2} current density for 5000 cycles is shown in Figure 6(c). The capacitance retention for S2 electrode (65%) is higher in comparison to S1 (51%) and S3 (44%) as shown in Figure 6(c). These results indicate the higher electrochemical cycling stability of S2 composite electrode. Figure 6(d) shows the Ragone plot of energy density vs. power density of the SC with S2 electrode. The energy density of 820 mWh cm^{-2} and the power density of 4.10 W cm^{-2} were obtained for the S2 electrode. Similar work was reported by Barik et al., which is found to have the energy density of 80 mWh cm^{-2} and power density of 4.87 W cm^{-2} for SnO_2@carbon nanofiber synthesized by the electrospinning method [45]. The schematic for the possible mechanism involved in the SnO_2/N-GQD NT composite electrodes during charge-discharge process is shown in Figure 7.

The schematic mechanism (Figure 7) shows the movement of ions in electrolyte during the charge-discharge process of the SnO_2/N-GQD NT electrodes. The K^+ and OH^- ions in the electrolyte move towards the opposite charged electrodes. The electrons in the OH^- ions adsorbed onto the surface of SnO_2/N-GQD electrodes undergo chemical reactions as discussed above in Equations (4) and (5). Whereas the K^+ ions adsorbed on the surface of the electrodes take electron released during SnO_2 reversible reactions and form an EDL during the charge process, in the charging process, both EDL and reversible chemical reactions both occur at the surface of the electrodes. The reversible reactions during the discharge process will retain the ionic combination of electrolyte resulting in neutral bulk electrolyte. The performance enhancement of S2 electrodes can be attributed to spacer effect of SnO_2 particles in the NTs incorporated with N-GQDs. The highly reversible faradaic redox process of SnO_2 also enhances the performance of SCs. The specific capacitance performance of the S2 electrode was higher in comparison to S1 and S3 and might be due to the factors discussed above such as spacer effect, good conductivity of N-GQDs, and good internal contacts between SnO_2 particles

and N-GQDs in the NTs. In the case of S1 electrodes, there are no additional conducting agents such as N-GQDs, whereas for S3 electrode, the N-GQDs concentration has hindered the adhesive property between SnO_2 crystals leading to damage of NT structures subsequently losing the conductivity advantage. In contrast, S2 has shown a good structural stability and enhanced conductivity for electrodes along with more suitable sites for the surface chemical reactions on SnO_2, therefore resulted as a good performing electrode than others.

From the above experimental results, the N-GQDs incorporated SnO_2 NTs have shown a considerable better improvement in the areal capacitance of the SnO_2 NTs due to the enhanced electrons and ionic diffusion with increase of more active sites. The moderate (3 wt.%) addition of N-GQDs into SnO_2 NTs has demonstrated an excellent electrochemical behavior due to the tubular porous morphology along with decrease in electrical resistance compared to pure SnO_2 NTs and higher N-GQDs containing samples. The improved capacitive behavior could be attributed to the decrease in the resistance of the electrodes and increase in the ionic diffusion from the bulk electrolyte solution to the surface of the electrodes due to the incorporation of N-GQDs. Based on these above studies, it is evident that SnO_2 NTs and N-GQDs composites are one of the good futuristic materials for the energy storage and conversion application and in many other interdisciplinary fields.

4. Conclusions

In summary, a simple and cost-effective one-step electrospinning technique followed by thermal annealing was adopted for the fabrication of pristine and N-GQDs incorporated SnO_2 NTs. The structural, morphology, and elemental studies of as-prepared samples were analyzed by different techniques. The combination of tubular microstructures, chemical stability, and electrochemical properties of the S2 (SnO_2/N-GQDs-3 wt.%) composite showed a good performance as an electrode in the supercapacitor device. This work demonstrates a simple and facile synthesis method for the preparation of SnO_2 NTs and their composites that can be efficiently used in the energy storage and conversion applications.

Data Availability

The data used to support the findings of this study are included in the article.

Conflicts of Interest

The authors declare that they have no conflicts of interest.

Acknowledgments

This research was supported by the Basic Science Research Program through the National Research Foundation of Korea (NRF) funded by the Ministry of Education (2018R1A6A1A03023788, 2021R1I1A1A01055790, and 2022R1I1A1A01070368) and the Korea Institute for Advancement of Technology (KIAT) grant funded by the Korean Government (MOTIE) (P00008500, the Competency Development Program for Industry Specialist). This research was also supported by the R&D Program of Ministry of Culture, Sports and Tourism and Korea Creative Content Agency (Development of K-Black Ink containing the Traditional Muk Material and its use in Digital Printing Technology, Project Number: R2020040047).

References

[1] Y. Zhang, S. Yu, G. Lou et al., "Review of macroporous materials as electrochemical supercapacitor electrodes," *Journal of Materials Science*, vol. 52, no. 19, pp. 11201–11228, 2017.

[2] R. Dubey and V. Guruviah, "Review of carbon-based electrode materials for supercapacitor energy storage," *Ionics*, vol. 25, no. 4, pp. 1419–1445, 2019.

[3] S. C. Shin, J. Kim, J. K. R. Modigunta et al., "Bio-mimicking organic-inorganic hybrid ladder-like polysilsesquioxanes as a surface modifier for polyethylene separator in lithium-ion batteries," *Journal of Membrane Science*, vol. 620, p. 118886, 2021.

[4] S. Najib and E. Erdem, "Current progress achieved in novel materials for supercapacitor electrodes: mini review," *Nanoscale Advances*, vol. 1, no. 8, pp. 2817–2827, 2019.

[5] U. Male, J. K. R. Modigunta, and D. S. Huh, "Design and synthesis of polyaniline-grafted reduced graphene oxide via azobenzene pendants for high-performance supercapacitors," *Polymer*, vol. 110, pp. 242–249, 2017.

[6] B. Zhao, D. Chen, X. Xiong et al., "A high-energy, long cycle-life hybrid supercapacitor based on graphene composite electrodes," *Energy Storage Materials*, vol. 7, pp. 32–39, 2017.

[7] C. Portet, P. L. Taberna, P. Simon, E. Flahaut, and C. Laberty-Robert, "High power density electrodes for carbon supercapacitor applications," *Electrochimica Acta*, vol. 50, no. 20, pp. 4174–4181, 2005.

[8] G. Murali, J. Rawal, J. K. R. Modigunta et al., "A review on MXenes: new-generation 2D materials for supercapacitors," *Sustainable Energy & Fuels*, vol. 5, no. 22, pp. 5672–5693, 2021.

[9] S. Jeon, J. H. Jeong, H. Yoo, H. K. Yu, B.-H. Kim, and M. H. Kim, "RuO2 nanorods on electrospun carbon nanofibers for supercapacitors," *ACS Applied Nano Materials*, vol. 3, no. 4, pp. 3847–3858, 2020.

[10] D. Majumdar, T. Maiyalagan, and Z. Jiang, "Recent progress in ruthenium oxide-based composites for supercapacitor applications," *ChemElectroChem*, vol. 6, no. 17, pp. 4343–4372, 2019.

[11] J. Cheng, B. Zhao, W. Zhang et al., "High-performance supercapacitor applications of NiO-nanoparticle-decorated millimeter-long vertically aligned carbon nanotube arrays via an effective supercritical CO2-assisted method," *Advanced Functional Materials*, vol. 25, no. 47, pp. 7381–7391, 2015.

[12] V. Bonu, B. Gupta, S. Chandra, A. Das, S. Dhara, and A. K. Tyagi, "Electrochemical supercapacitor performance of SnO_2 quantum dots," *Electrochimica Acta*, vol. 203, pp. 230–237, 2016.

[13] D. Wu, X. Xie, Y. Zhang et al., "MnO_2/carbon composites for supercapacitor: synthesis and electrochemical performance," *Frontiers in Materials*, vol. 7, no. 2, 2020.

[14] L. Demarconnay, E. Raymundo-Piñero, and F. Béguin, "Adjustment of electrodes potential window in an asymmetric

carbon/MnO2 supercapacitor," *Journal of Power Sources*, vol. 196, no. 1, pp. 580–586, 2011.

[15] S. Xu, L. You, P. Zhang, Y. Zhang, J. Guo, and C. Wang, "Fe_3O_4@coordination polymer microspheres with self-supported polyoxometalates in shells exhibiting high-performance supercapacitive energy storage," *Chemical Communications*, vol. 49, no. 24, pp. 2427–2429, 2013.

[16] C. Xue, Y. Lv, F. Zhang, L. Wu, and D. Zhao, "Copper oxide activation of soft-templated mesoporous carbons and their electrochemical properties for capacitors," *Journal of Materials Chemistry*, vol. 22, no. 4, pp. 1547–1555, 2012.

[17] T. Lu, L. Pan, H. Li et al., "Microwave-assisted synthesis of graphene–ZnO nanocomposite for electrochemical supercapacitors," *Journal of Alloys and Compounds*, vol. 509, no. 18, pp. 5488–5492, 2011.

[18] C.-A. Tseng, P. K. Sahoo, C.-P. Lee, Y.-T. Lin, J.-H. Xu, and Y.-T. Chen, "Synthesis of CoO-decorated graphene hollow nanoballs for high-performance flexible supercapacitors," *ACS Applied Materials & Interfaces*, vol. 12, no. 36, pp. 40426–40432, 2020.

[19] C. E. Shuck, M. Han, K. Maleski et al., "Effect of Ti3AlC2MAX phase on structure and properties of resultant Ti3C2TxMXene," *ACS Applied Nano Materials*, vol. 2, no. 6, pp. 3368–3376, 2019.

[20] S. R. Ch, L. Zhang, Y. Qiu, Y. Chen, and S. R. Dugasani, "Investigation of hydrogen sensing properties of graphene/Al- SnO_2 composite nanotubes derived from electrospinning," *Journal of Industrial and Engineering Chemistry*, vol. 63, pp. 411–419, 2018.

[21] J. C. Briones, G. Castillon, M. P. Delmo, and G. N. C. Santos, "Magnetic-field-enhanced morphology of tin oxide nanomaterials for gas sensing applications," *Journal of Nanomaterials*, vol. 2017, Article ID 4396723, 11 pages, 2017.

[22] S. Choudhury, R. Nautiyal, D. K. Thakkar, and C. A. Betty, "Thickness dependence of nanocrystalline tin oxide thin films in capacitive biosensor characterization," *Journal of Electroanalytical Chemistry*, vol. 877, p. 114742, 2020.

[23] A. Gabriunaite, T. S. Valiūnienė, and G. Valincius, "Mixed silane-based self-assembled monolayers deposited on fluorine doped tin oxide as model system for development of biosensors for toxin detection," *Electroanalysis*, vol. 33, no. 5, pp. 1315–1324, 2021.

[24] Z. Guo, A. K. Jena, I. Takei et al., "VOC over 1.4 V for amorphous tin-oxide-based dopant-free $CsPbI_2Br$ perovskite solar cells," *Journal of the American Chemical Society*, vol. 142, no. 21, pp. 9725–9734, 2020.

[25] J. A. Smith, O. S. Game, J. E. Bishop et al., "Rapid scalable processing of tin oxide transport layers for perovskite solar cells," *ACS Applied Energy Materials*, vol. 3, no. 6, pp. 5552–5562, 2020.

[26] M. J. K. Reddy, S. H. Ryu, and A. M. Shanmugharaj, "Synthesis of SnO_2 pillared carbon using long chain alkylamine grafted graphene oxide: an efficient anode material for lithium ion batteries," *Nanoscale*, vol. 8, no. 1, pp. 471–482, 2016.

[27] F. Zoller, D. Böhm, T. Bein, and D. Fattakhova-Rohlfing, "Tin oxide based nanomaterials and their application as anodes in lithium-ion batteries and beyond," *ChemSusChem*, vol. 12, no. 18, pp. 4140–4159, 2019.

[28] J. C. M. Brokken-Zijp, O. L. J. van Asselen, W. E. Kleinjan, R. van de Belt, and G. de With, "Photocatalytic properties of tin oxide and antimony-doped tin oxide nanoparticles," *Journal of Nanotechnology*, vol. 2011, Article ID 106254, 15 pages, 2011.

[29] C. Mevada and M. Mukhopadhyay, "Electrochemical performance of aqueous asymmetric supercapacitor based on synthesized tin oxide positive and commercial titanium dioxide negative electrodes," *Journal of Energy Storage*, vol. 33, p. 102058, 2021.

[30] R. Kumar, R. K. Nekouei, and V. Sahajwalla, "In-situ carbon-coated tin oxide (ISCC-SnO2) for micro-supercapacitor applications," *Carbon Letters*, vol. 30, no. 6, pp. 699–707, 2020.

[31] B. Varshney, M. J. Siddiqui, A. H. Anwer et al., "Synthesis of mesoporous SnO_2/NiO nanocomposite using modified sol-gel method and its electrochemical performance as electrode material for supercapacitors," *Scientific Reports*, vol. 10, no. 1, p. 11032, 2020.

[32] V. Velmurugan, U. Srinivasarao, R. Ramachandran, M. Saranya, and A. N. Grace, "Synthesis of tin oxide/graphene (SnO_2/G) nanocomposite and its electrochemical properties for supercapacitor applications," *Materials Research Bulletin*, vol. 84, pp. 145–151, 2016.

[33] R. B. Rakhi, W. Chen, D. Cha, and H. N. Alshareef, "High performance supercapacitors using metal oxide anchored graphene nanosheet electrodes," *Journal of Materials Chemistry*, vol. 21, no. 40, pp. 16197–16204, 2011.

[34] H. M. Jeong, K. M. Choi, T. Cheng et al., "Rescaling of metal oxide nanocrystals for energy storage having high capacitance and energy density with robust cycle life," *Proceedings of the National Academy of Sciences*, vol. 112, no. 26, pp. 7914–7919, 2015.

[35] X. Lu, C. Wang, F. Favier, and N. Pinna, "Electrospun nanomaterials for supercapacitor electrodes: designed architectures and electrochemical performance," *Advanced Energy Materials*, vol. 7, no. 2, p. 1601301, 2017.

[36] K.-A. Tsai, P.-Y. Hsieh, T.-H. Lai et al., "Nitrogen-doped graphene quantum dots for remarkable solar hydrogen production," *ACS Applied Energy Materials*, vol. 3, no. 6, pp. 5322–5332, 2020.

[37] S. Kang, Y. K. Jeong, J. H. Ryu et al., "Pulsed laser ablation based synthetic route for nitrogen-doped graphene quantum dots using graphite flakes," *Applied Surface Science*, vol. 506, p. 144998, 2020.

[38] G. Murali, M. Reddeppa, C. Seshendra Reddy et al., "Enhancing the charge carrier separation and transport via nitrogen-doped graphene quantum Dot-TiO_2 nanoplate hybrid structure for an efficient NO gas sensor," *ACS Applied Materials & Interfaces*, vol. 12, no. 11, pp. 13428–13436, 2020.

[39] S. Zhang, Y. Li, H. Song et al., "Graphene quantum dots as the electrolyte for solid state supercapacitors," *Scientific Reports*, vol. 6, no. 1, p. 19292, 2016.

[40] C. S. Reddy, G. Murali, A. S. Reddy, S. Park, and I. In, "GO incorporated SnO_2 nanotubes as fast response sensors for ethanol vapor in different atmospheres," *Journal of Alloys and Compounds*, vol. 813, p. 152251, 2020.

[41] L. Tang, R. Ji, X. Li, K. S. Teng, and S. P. Lau, "Energy-level structure of nitrogen-doped graphene quantum dots," *Journal of Materials Chemistry C*, vol. 1, no. 32, pp. 4908–4915, 2013.

[42] S. Raj, P. Kar, and P. Roy, "Ammonia-assisted growth of CoSn(OH)6 nanostructures and their electrochemical performances for supercapacitor," *Journal of Nanoscience and Nanotechnology*, vol. 19, no. 5, pp. 2755–2761, 2019.

[43] R. N. Bulakhe, S. A. Arote, B. Kwon, S. Park, and I. In, "Facile synthesis of nickel cobalt sulfide nano flowers for high performance supercapacitor applications," *Materials Today Chemistry*, vol. 15, p. 100210, 2020.

[44] K.-K. Liu, Q. Jiang, C. Kacica, H. G. Derami, P. Biswas, and S. Singamaneni, "Flexible solid-state supercapacitor based on tin oxide/reduced graphene oxide/bacterial nanocellulose," *RSC Advances*, vol. 8, no. 55, pp. 31296–31302, 2018.

[45] R. Barik, V. Tanwar, R. Kumar, and P. P. Ingole, "A high energy density and high rate capability flexible supercapacitor based on electro-spun highly porous SnO_2@carbon nanofibers," *Journal of Materials Chemistry A*, vol. 8, no. 30, pp. 15110–15121, 2020.